International Journal of Advanced Structural Engineering, Vol. 1, No. 1, Pages 53-76, July 2009
Islamic Azad University, South Tehran Branch

SEISMIC ASSESSMENT AND STRENGTHENING OF AN EXISTING STEEL BRIDGE IN PORTUGAL

Catarina Fernandes[1] and Humberto Varum[2]
Department of Civil Engineering, University of Aveiro, Aveiro, Portugal

Received 12 January 2009
Revised 16 February 2009
Accepted 19 March 2009

This article presents the seismic vulnerability assessment of the S. João de Loure bridge, in Portugal. The single span steel bridge has riveted joints, commonly affected by corrosion, which can lead to a significant stiffness reduction. With the objective of evaluating the influence of the joints stiffness in the structural response of the bridge, a structural model of the bridge was created, and natural frequencies, maximum axial forces and maximum stresses, and maximum mid-span deflection were analysed. Four possible element rupture scenarios where also studied. Two of them where proved to be a risk for the structural safety of the bridge. A commonly used strengthening solution intending to reduce the bridge's mid-span deflection with external pre-stressing cables was studied.

Keywords: existing steel bridge, joint stiffness, vulnerability assessment, rupture scenarios, strengthening solution

1. Introduction

The deterioration of existing bridge structures results mainly of wrong dimensioning, unsatisfactory construction and installation of components and inadequate mechanical loads due to traffic, temperature, etc. Global stability can be particularly affected by corrosion (Nóvak et al. 2005). To prevent theirs deterioration, periodical maintenance operations should be performed. Its crucial role in the preservation of structures is not always taken into account and maintenance is not always performed attending to appropriate standards and regulations. As a result, the structural safety of structures and the safety of its users can not always be assured.

[1] Ph.D. Student
[2] Assistant Professor

Corrosion is one of the most common problems in steel structures. Regarding steel bridges, its joints are very vulnerable to this pathology. First, the chemical composition of the joint elements is usually different from the chemical composition of the steel elements which they connect. Second, the region of connection between elements is commonly affected by humidity. Among other factors, these two can justify the high risk of corrosion of joint elements. As a consequence of corrosion, the joints cross-section is reduced (and its axial stiffness) and the possibility of the bridge safety can no longer be satisfied should be considered. Having this in mind, one of the objectives of this work was to evaluate the influence of the joints stiffness in the structural response of the S. João de Loure steel bridge. Natural frequencies corresponding to the most significant vibration modes, maximum axial forces and maximum stresses in the elements of the bridge, and maximum bridge deflection, were analysed.

The rupture of an element of a bridge can result from their insufficient strength, insufficient buckling strength of the elements under compression, corrosion, vehicles collision, etc. Simulating bars rupture scenarios and analysing its consequences in the global structural behaviour and safety of the bridge was the second objective of this work.

Finally, a common strengthening solution with pre-stressing cables was studied, intending to reduce the bridge's mid-span deflection.

The structural analysis software SAP2000 (2003) was used to perform all the numerical analyses within this work.

2. Description of the Bridge

The S. João de Loure bridge under analysis (Figure 1) is located in S. João de Loure, district of Aveiro, Portugal, and it is a part of the national highway EN 230-2.

It is a steel bridge and the material properties adopted for all the numerical analyses presented in this paper are summarized in Table 1. The material properties have to be well estimated because the values adopted in the design of the structures normally do not correspond to their actual condition. In this case, the values presented in Table 1 are based in experimental test results on similar structures and correspond to the ones mentioned in a previous study about this bridge, by Furtado and Marques (2003).

Table 1. Steel properties (Furtado and Marques, 2003)

Characteristic yielding stress f_{yk}	Characteristic ultimate stress f_{uk}	Young's modulus E
225 MPa	245 MPa	200 GPa

Figure 1. General view of the S. João de Loure bridge (Furtado et al., 2003)

The bridge has a single span with approximately 43.36 m. Eleven panels can be identified, each with a length of 3.54 m. Table 2 summarizes the main geometrical characteristics of the bridge. The connection between elements is assured by rivets, as shown in Figure 2. The main structure is supported by two different types of bearings located in masonry abutments: fixed supports in the north abutment (Figure 3) and roller bearings in the south one. At the level of the bottom flanges, a bracing system guarantees the protection against lateral torsional buckling (Figure 4).

Table 2. Geometrical characteristics of the structure (Freire et al., 1998; Furtado et al., 2003)

Number of spans	1
Span length	43.36 m
Steel deck length	44.00 m
Road width	4.40 m
Footways width	2×0.80 m
Bridge girders height	4.35 m
Bridge girders spacing	6.00 m

(a) (b) (c)

Figure 2. Joint elements: a) Cross-girder/stringer; b) Main girder/stringer; c) Diagonal/flange/post

Figure 3. Fixed support in the north abutment (Furtado et al., 2003)

Figure 4. Bottom views of the S. João de Loure bridge: bracing system (Furtado et al., 2003)

3. Analytical Model

3.1. General Description

A 3D structural model of the bridge (see Figure 5) was built on SAP2000 (2003). The Finite Element Method (FEM) is widely used to accomplish numerical analyses. The model created for the S. João de Loure bridge is exclusively composed by bar elements, representing the steel structural elements, and it is an improvement of a model previously created by Furtado and Marques (2003). Flanges and cross-girders were considered continuous due to theirs characteristics and high stiffness of its joints. Diagonals, posts, stringers and bracing elements were considered hinged at the extremities.

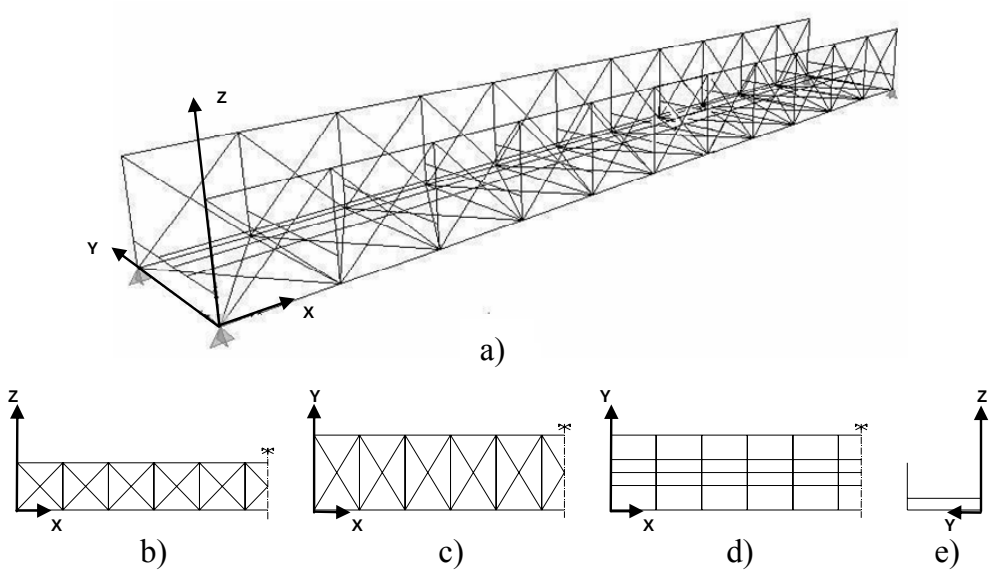

Figure 5. General geometry of the structural model: a) 3D view; b) XOZ view; c) XOY view, level of the bracing elements; d) XOY view, level of the cross-girders and stringers; e) YOZ view

Aiming at the evaluation of the joints stiffness influence in the global structural response of the S. João de Loure bridge, diagonals and posts were modelled in three sub-elements. Each bar of length L representing the diagonals was divided in three sub-elements (Figure 6): one central sub-element with length L' and two external sub-elements, each with length L_j. The external sub-elements intend to represent the joints and its length L_j was calculated from the AutoCAD drawings (2001). The same procedure was adopted for the posts, but four sub-elements had to be considered because an additional node was necessary to apply the loads from the cross-girder. Therefore, the central sub-element was divided in two.

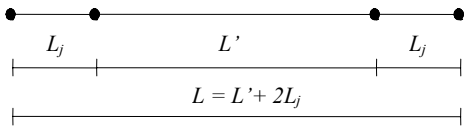

Figure 6. Improved model: consideration of 3 sub-elements

3.2. Geometrical Properties of the Element's Cross-section

The geometry of the cross-sections is quite complex. Therefore, the geometrical characteristics of the elements cross-sections area, centre of gravity and moments of inertia were calculated from

the AutoCAD drawings (2001) and are summarily presented in Table 3. The coordinate axes used for the computation were considered centred in the left inferior point of each cross-section: axis *y* corresponds to the horizontal axis and axis *z* to the vertical one. All bars have a uniform cross-section along its length.

The nomenclature adopted for the cross-sections is shown in Figure 7. Figure 8 shows examples of the geometry of some elements cross-sections.

Table 3. Geometrical characteristics of the element's cross-sections

Bridge elements	Label	Area	Centre of Gravity		Moment of Inertia	
		A (m^2)	z_G (m)	y_G (m)	I_{zG} (cm^4)	I_{yG} (cm^4)
Flanges	*FL 1*	0.015870	0.1183	0.2250	9489	36987
	FL 2	0.020820	0.0999	0.2250	17842	42779
	FL 3	0.025770	0.0907	0.2250	26196	47228
	FL 4	0.025770	0.0862	0.2250	34549	51072
Diagonals	*DIAG 1*	0.009823	0.0259	0.1775	16636	811
	DIAG 2	0.006510	0.0265	0.1500	8230	561
	DIAG 3	0.004680	0.0210	0.1300	4196	293
	DIAG 4	0.004076	0.0218	0.1100	2769	225
Posts	*POST 1*	0.029408	0.2564	0.2243	84353	37808
	POST 2	0.027096	0.2297	0.2145	80994	11608
	POST 3	0.005848	0.1542	0.0750	234	12753
	POST 4	0.003600	0.0491	0.0750	233	932
Cross-girders	*CGIRD*	0.023284	0.3950	0.0985	1497	173655
Stringers	*STRIN*	0.009600	0.2000	0.0890	968	24316
Bracing elements	*BRAC 1*	0.002122	0.0205	0.0710	188	98
	BRAC 2	0.001061	0.0205	0.0205	49	49

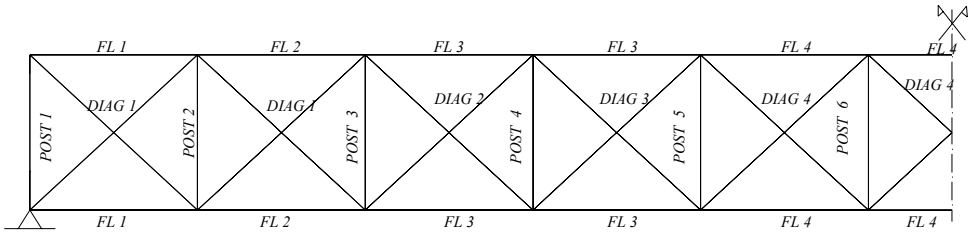

Figure 7. Cross-section's nomenclature: diagonals, posts and flanges

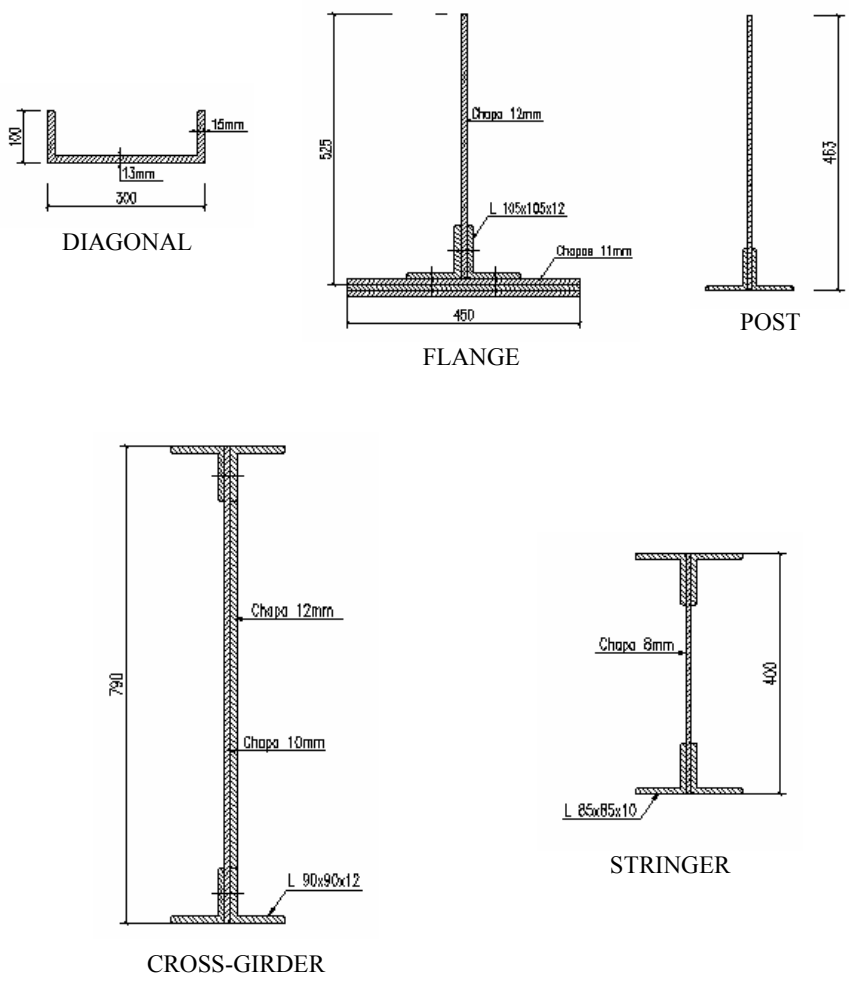

Figure 8. Examples of the element's cross-sections

3.3. Loads and Load Combinations

The dead loads, *G*, considered in the analyses are presented in Table 4. The weight of the steel structure was automatically evaluated by SAP2000 (2003) and multiplied by 1.1 to account for the fastenings weight (gusset's plates, weldings and rivets). The values adopted for the materials density were 77 kN/m^3 for the steel and 25 kN/m^3 for the concrete.

The live loads considered were calculated according to the Portuguese National Standard (RSA 1983), for class I highway bridges (see Table 4). In this preliminary assessment, the loads corresponding to wind and earthquake actions were not taken into account.

Table 4. Loads acting on the structure

Dead Loads	Live Loads (RSA)
Weight of the steel structure	Load of 4 kN/m^2 (Q_{distr}) uniformly distributed over the deck, plus a transversal load of 50 kN/m acting on every possible position of the deck
Weight of the concrete slab deck, footways and bridge rails	Or vehicle-type ($Q_{vehicle}$), acting on every possible position of the deck
	Load of 3 kN/m^2 uniformly distributed on the footways, or concentrated load of 20 kN ($Q_{footway}$) acting on the bridge rails

Regarding the load combinations, two ultimate limit state combinations were considered (ULT 1 and ULT 2), as explained in the following:

$$\text{ULT 1: } 1.35G + 1.5\left(Q_{vehicle} + Q_{footway}\right) \tag{1}$$

$$\text{ULT 2: } 1.35G + 1.5\left(Q_{distr} + Q_{footway}\right) \tag{2}$$

For each load combination (1 and 2), different positions for the loads were considered: four positions for the vehicle-type ($Q_{vehicle}$) in ULT 1, and two positions for the transversal load (Q_{distr}) in ULT 2.

Concerning the serviceability limit state, the bridge was analysed for two combinations:

$$\text{SERV 1: } G + \psi_1\left(Q_{vehicle} + Q_{footway}\right),\ \psi_1 = 0.4 \tag{3}$$

$$\text{SERV 2: } G + \psi_1\left(Q_{distr} + Q_{footway}\right),\ \psi_1 = 0.4 \tag{4}$$

In the serviceability limit state combinations, both the vehicle-type and the transversal load were applied at the mid-span, corresponding to the more severe situation in terms of bridge deflection. For the vehicle-type, two different loading positions were considered, namely the vehicle-type centred in the bridge's cross-section (SERV 1-A) and vehicle-type with maximum eccentricity in the bridge's cross-section (SERV 1-B).

4. Influence of the Joints Stiffness in the Structural Response

As previously stated, each diagonal and each post were modelled with three general sub-elements, with the two external ones representing the joints in the corresponding element. In order to evaluate the influence of the joints stiffness in the global response of the bridge, it was

necessary to simulate the variation of theirs stiffness. With this purpose, to the external sub-elements were attributed various axial stiffnesses EA_{NL} (E for the Young's modulus and A for the cross-section's area), as shown in Figure 9. The axial stiffness varies in the range (0.5EA; 1.5EA), where EA represents the nominal axial stiffness of the central sub-element. The variations considered simulate, on one hand, possible reductions of the cross-section's area of the joints, which can be caused by, for example, corrosion. On the other hand, to simulate stiffening of the joints due to the fabrication (gussets, etc.), the structural response was analysed for joints stiffness values bigger than the nominal one. The structural response was then evaluated for the following values of EA_{NL}: 0.5EA, 0.6EA, 0.7EA, 0.8EA, 0.9EA, 1.0EA, 1.1EA, 1.2EA, 1.3EA, 1.4EA and 1.5EA. Natural frequencies, maximum axial forces and corresponding stress in the elements, and maximum deflection, were analysed for each stiffness value.

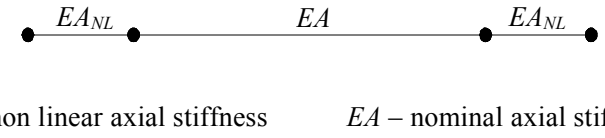

Figure 9. Consideration of non-linear axial stiffness for the lateral sub-elements

4.1. Numerical Results

4.1.1. Natural Frequencies

The analysis was made for the first 16 most significant vibration modes. Table 5 describes the vibration modes and presents the corresponding natural frequencies of the structure. Since the natural frequencies did not show a significant variation for each value of EANL under analysis, the frequencies presented are the ones calculated for EANL = EA and can be considered valid for all the values of EANL in the range (0.5EA; 1.5EA).

4.1.2. Maximum Axial Force and Maximum Stress

Table 6 presents the maximum axial forces, Nmax, and maximum stresse, σmax, in the elements, calculated for the ultimate limit state combinations. The location of the elements where the maximum stress occurs is shown in Figure 10. Diagonal and flanges with maximum axial force correspond to the ones with maximum stress, but the post with maximum force is not the post with maximum stress.

Table 5. Vibration modes and corresponding frequencies

	Vibration modes		Frequencies (Hz)
1	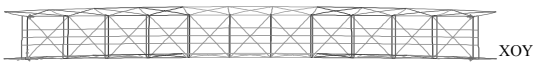 XOY	Transversal bending of the overall structure	2.12
2	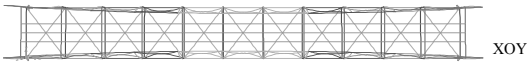 XOY	Transversal bending of the main girders	2.97
3 – 13	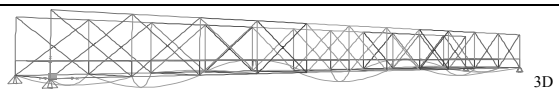 3D	Local bending of the bracing elements	3.03
14	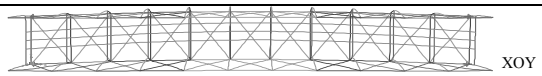 XOY	Transversal bending of the overall structure	3.90
15	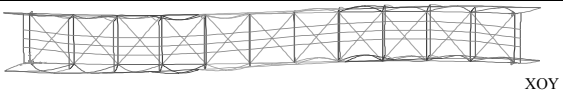 XOY	Transversal bending of the overall structure	5.03
16	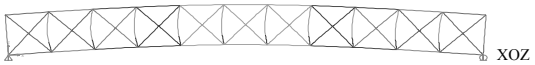 XOZ	In-plane bending of the overall structure	5.18

Table 6. Maximum axial forces and corresponding stress

	Diagonal		Post		Upper flange		Bottom flange	
EA_{NL}/EA	N_{max} (kN)	σ_{max} (MPa)	N_{max} (kN)	σ_{max} (MPa)	N_{max} (kN)	σ_{max} (MPa)	N_{max} (kN)	σ_{max} (MPa)
0.5	-855.44	-174.17	-690.13	-86.45	-3401.44	-131.99	3300.13	128.06
0.6	-854.95	-145.06	-690.79	-72.63	-3406.27	-132.18	3302.16	128.14
0.7	-854.52	-124.27	-691.32	-62.66	-3409.84	-132.32	3303.80	128.20
0.8	-854.15	-108.69	-691.75	-55.12	-3412.59	-132.42	3305.00	128.25
0.9	-853.83	-96.58	-692.11	-49.20	-3414.77	-132.51	3305.90	128.28
1	-853.56	-86.89	-692.42	-44.44	-3416.55	-132.58	3306.61	128.31
1.1	-853.31	-78.97	-692.68	-40.53	-3418.02	-132.64	3307.17	128.33
1.2	-853.10	-72.37	-692.90	-37.25	-3419.27	-132.68	3307.63	128.35
1.3	-852.92	-66.79	-693.10	-34.46	-3420.33	-132.73	3308.01	128.37
1.4	-852.75	-62.01	-693.27	-32.06	-3421.26	-132.76	3308.33	128.38
1.5	-852.60	-57.86	-693.42	-29.98	-3422.06	-132.79	3308.60	128.39

The maximum stress surges at the diagonal and for $EA_{NL} = 0.5EA$, and is equal to 174.17 MPa. Therefore, the structural safety is verified according to the Portuguese standards (REAE 1986) for all the elements and for all the values of EA_{NL} analysed. Note that the effect of local or global instability was not considered.

$$\sigma_{max} = 174.17 \text{ MPa} < f_{yd} = f_{yk} / 1.1 = 225/1.1 = 204.55 \text{ MPa} \tag{5}$$

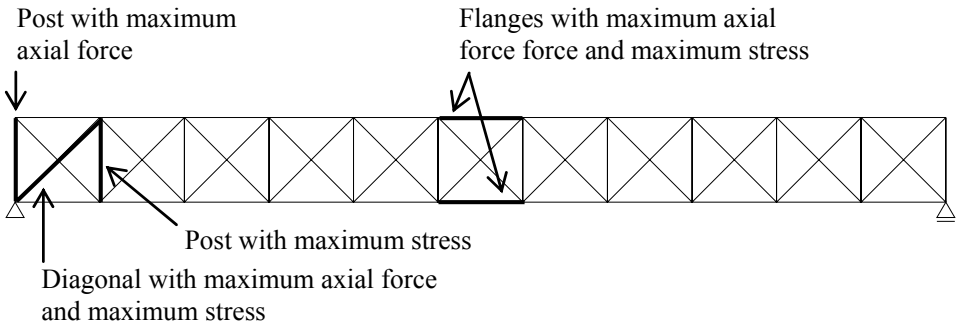

Figure 10. Location of the elements with maximum axial force and maximum stress

The evolution of the maximum axial force and maximum stress for each element, function of the axial stiffness, is shown in Figures 11 and 12, respectively.

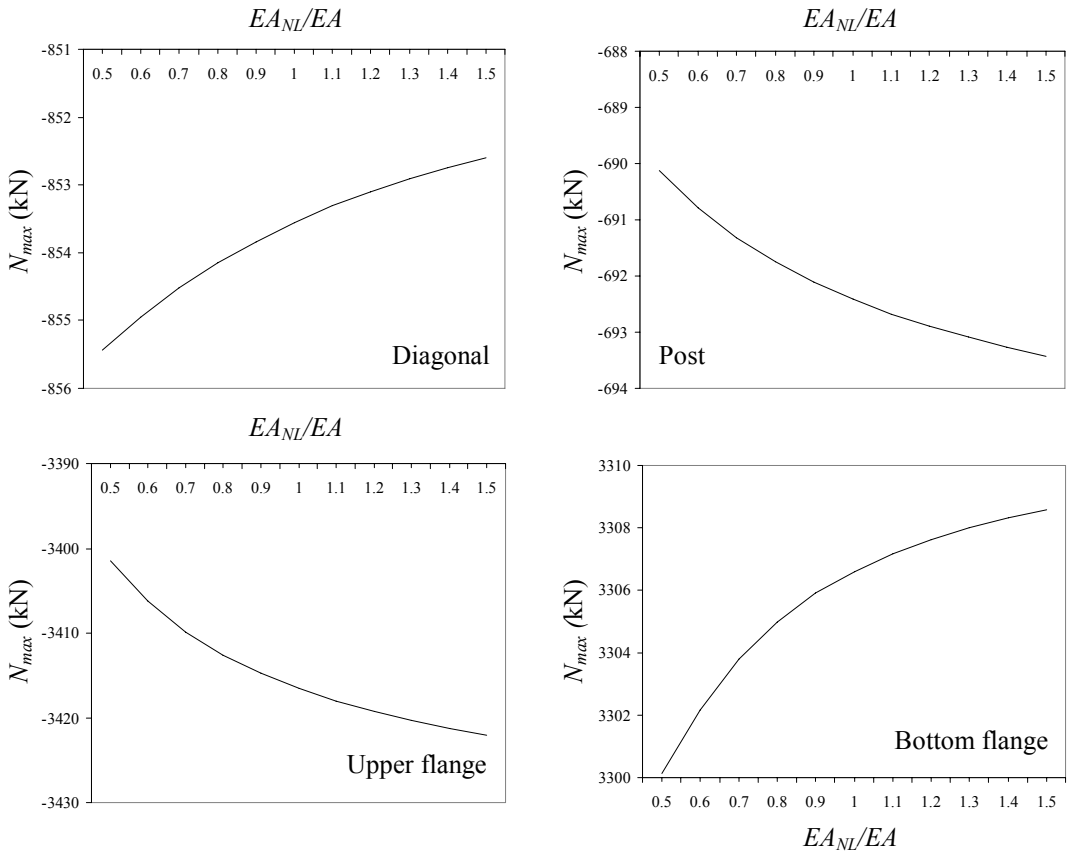

Figure 11. Maximum axial forces in the elements function of the axial stiffness

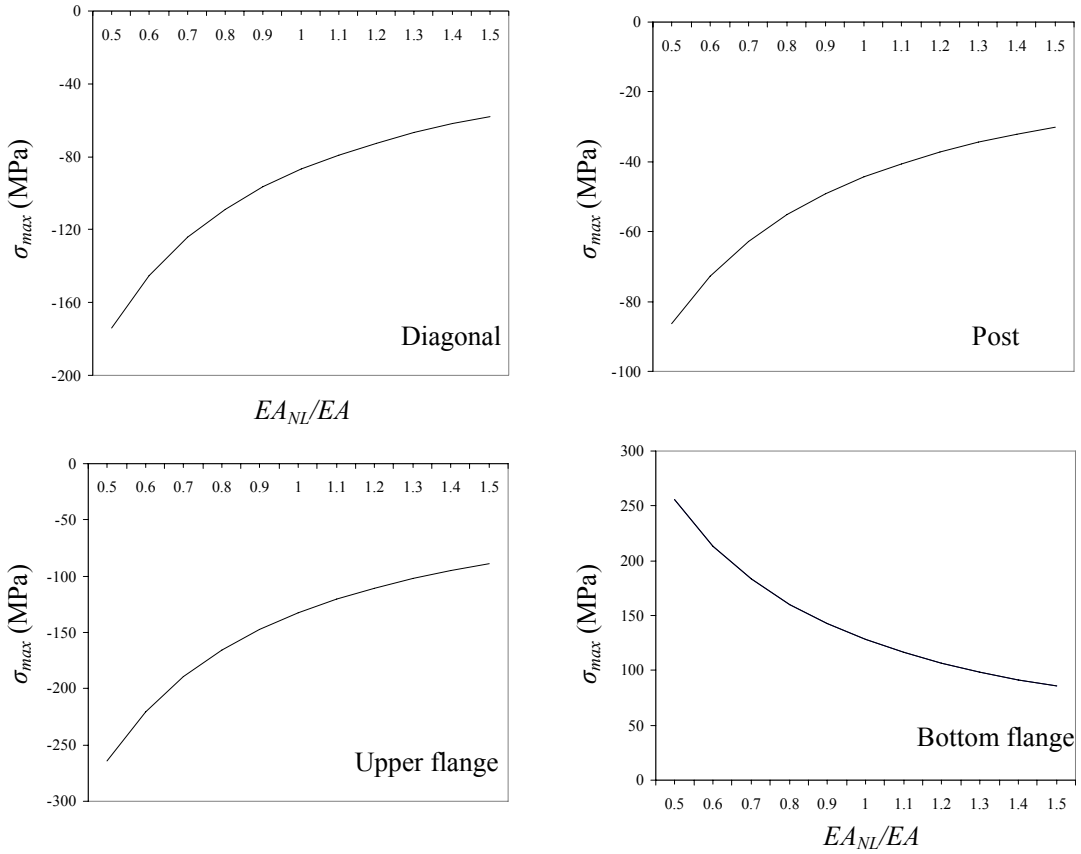

Figure 12. Maximum stress in the elements, function of the axial stiffness

4.1.3. Maximum Deflection

The maximum deflection, located at the mid-span, δ1/2span, was calculated for the serviceability limit state combinations. The combination SERV 2 gives the maximum values, as shown in Table 7 and in Figure 13.

Table 7. Maximum deflection

EA_{NL}/EA	$\delta_{1/2span}$ (cm)		
	SERV 1-A	SERV 1-B	SERV 2
0.5	4.38	4.26	4.42
0.6	4.32	4.20	4.35
0.7	4.28	4.16	4.31
0.8	4.25	4.12	4.28
0.9	4.22	4.10	4.25
1	4.20	4.08	4.23
1.1	4.18	4.06	4.21
1.2	4.17	4.05	4.20
1.3	4.16	4.04	4.19
1.4	4.15	4.02	4.18
1.5	4.14	4.02	4.17

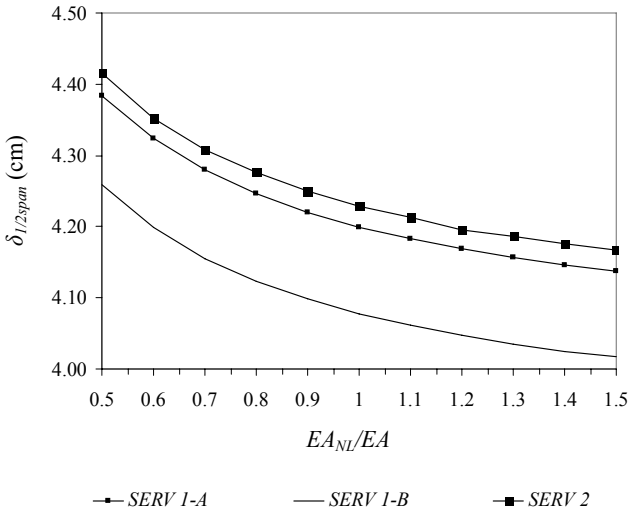

Figure 13. Maximum deflection, function of the axial stiffness

4.2. Discussion of the Results

As stated in section 4.1.1, the natural frequencies did not show a significant variation for the different values of the axial stiffness EA_{NL}. The first vibration mode corresponds to the global bending of the overall structure and the second to the transversal bending of the main girders. The associated natural frequencies are 2.12 Hz and 2.97 Hz, for the first and the second mode, respectively. Regarding the maximum axial forces and maximum stress in the elements, the most relevant results are the corresponding to a 50% reduction of the cross-section's area, i.e. for EA equal to $0.5EA_{NL}$. For this stiffness value and according to the results shown in section 4.1.2, the following variations can be observed:

- posts: maximum axial force reduced by 0.3% and corresponding stress increased by 95%

- upper flanges: maximum axial force and corresponding stress reduced by 0.4%

- bottom flanges: maximum axial force and corresponding stress reduced by 0.2%

- diagonals: maximum axial force increased by 0.2% and corresponding stress increased by 100%

The small variation of the axial forces is probably a consequence of the characteristics of the bridge. On one hand, the structure's behaviour is essentially isostatic. On the other hand, the diagonals and posts stiffness is significantly inferior than the flanges stiffness. Thus, the load distribution within the structure practically does not depend on the diagonals and posts stiffness.

Concerning the mid-span deflection, the maximum variation is equal to 4% (increase), for EA_{NL}/EA equal to 0.5. Only diagonals and posts were divided in sub-elements and the length of the external ones represented a small percentage of the total length of the element: 26% for the diagonals and 20% for the posts. This can justify the small variation of the mid-span deflection with the variation of theirs non-linear axial stiffness.

5. Rupture Scenarios

Insufficient strength, insufficient buckling strength of the elements under compression, corrosion, vehicles collision, etc., can cause the rupture of bridge elements. Having this in mind, four rupture scenarios were simulated corresponding to: rupture of a diagonal, rupture of a post, rupture of an upper flange and rupture of a bottom flange. In each case, the element where the rupture is simulated corresponds to the one with the higher stress in the previous assessment analysis, for the nominal axial stiffness (EA equal to EA_{NL}). To simulate the rupture of an element in the model, the corresponding element was subtracted (Figure 14).

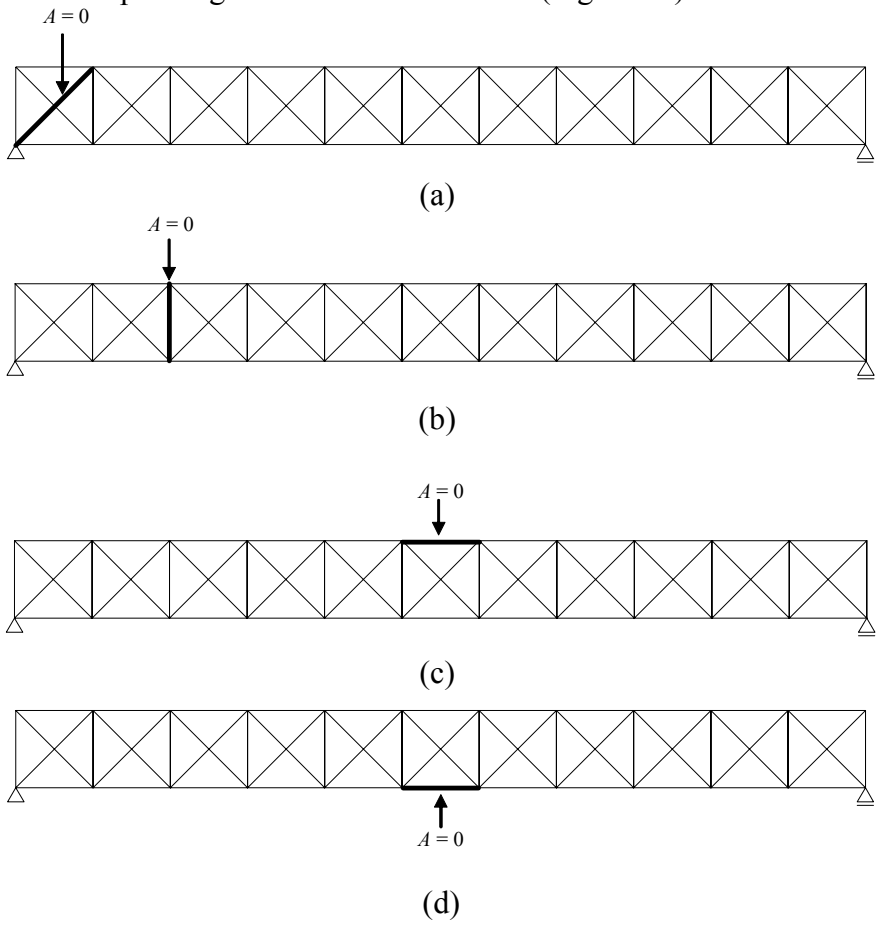

Figure 14. Rupture scenarios: a) Diagonal; b) Post; c) Upper flange; d) Bottom flange.

For each rupture scenario, natural frequencies, maximum axial forces and maximum stresses in the elements, and maximum deflection, were analysed.

5.1. Numerical Results

5.1.1. Natural Frequencies

The frequencies analysis was made for the first 16 vibration modes, as described in Table 8.

Table 8. Vibration modes and corresponding frequencies

Rupture scenario	Vibration mode		
	Mode	Description	Frequencie (Hz)
Diagonal	1	Transversal bending of the overall structure	2.12
	2	Transversal bending of the main girders	2.95
	3 – 13	Local bending of the bracing elements	3.03
	14	Transversal bending of the overall structure	3.90
	15	Transversal bending of the overall structure	5.03
	16	In-plane bending of the overall structure	5.15
Post	1	Local mode	0.86
	2	Transversal bending of the overall structure	2.12
	3	Transversal bending of main girders	3.01
	4 – 14	Local bending of the bracing elements	3.03
	15	Local mode	3.83
	16	Local mode	4.30
Upper flange	1	Transversal bending of the overall structure	2.17
	2 – 12	Local bending of the bracing elements	3.03
	13	Transversal bending of the main girders	3.06
	14	In-plane bending of the overall structure	3.64
	15	Transversal bending of the overall structure	3.93
	16	Transversal bending of the overall structure	5.03
Bottom flange	1	Transversal bending of the overall structure	2.03
	2	Transversal bending of the main girders	2.97
	3 – 13	Local bending of the bracing elements	3.03
	14	Transversal bending of the overall structure	3.53
	15	In-plane bending of the overall structure	4.39
	16	Transversal bending of the overall structure	5.03

5.1.2. Maximum Axial Forces and Maximum Stresses

Table 9 presents the maximum axial forces, N_{max}, and maximum stresses, σ_{max}, in the elements, calculated for each rupture scenario. In all scenarios, diagonals and flanges with maximum axial

force are the ones with maximum stress. Again, as verified in the previous assessment analysis, the post with maximum axial force does not correspond to the one with maximum stress (see Figure 10).

Table 9. Maximum axial forces and corresponding stress

	Elements with maximum stress			
Rupture scenario	Element	Label	N_{max} (kN)	σ_{max} (MPa)
Diagonal	Diagonal	*DIAG 1*	1599.54	162.84
	Post	*POST 1*	-1241.77	-42.43
	Upper flange	*FL 4*	-3436.04	-133.33
	Bottom flange	*FL 4*	3321.01	128.87
Post	Diagonal	*DIAG 1*	-1001.47	-101.95
	Post	*POST 3*	-452.86	-77.44
	Upper flange	*FL 4*	-3477.14	-134.93
	Bottom flange	*FL 4*	3307.41	128.34
Upper flange	Diagonal	*DIAG 4*	-2653.90	-651.10
	Post	*POST 3*	1534.62	262.42
	Upper flange	*FL 4*	4277.08	-165.97
	Bottom flange	*FL 4*	4010.11	155.61
Bottom flange	Diagonal	*DIAG 4*	1830.58	449.11
	Post	*POST 3*	-1373.97	-234.95
	Upper flange	*FL 4*	-3883.57	-150.70
	Bottom flange	*FL 4*	4562.70	177.05

The safety, as defined by expression (5), is verified in all bars for both the diagonal and post rupture scenarios. Regarding the rupture scenario of the upper and bottom flanges, in both cases the diagonals and posts with maximum stress, located in the central panel (Figure 15), do not verify the safety. For these two last modes, the safety factor for each element, calculated as the ratio between the characteristic acting stress and the characteristic yielding stress (expressions 6 to 9), shows that the diagonal with maximum stress will surely collapse as a consequence of the rupture of the upper or bottom middle flanges.

Rupture of the upper flange:

$$\sigma_{max,diagonal,k} \big/ f_{yk} = 465.07/225 = 2.07 \tag{6}$$

$$\sigma_{max,post,k} \big/ f_{yk} = 187.44/225 = 0.83 \tag{7}$$

Rupture of the bottom flange:

$$\sigma_{max,diagonal,k} / f_{yk} = 320.79/225 = 1.42 \quad (8)$$

$$\sigma_{max,post,k} / f_{yk} = 167.82/225 = 0.74 \quad (9)$$

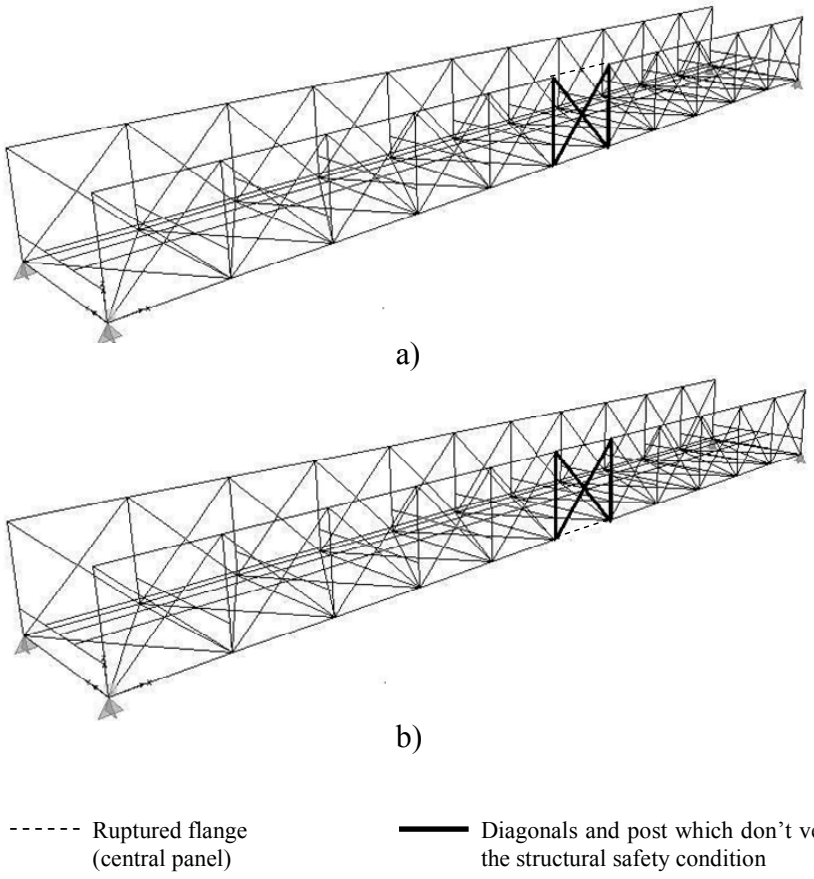

Figure 15. Diagonal and post which don't verify the structural safety condition: a) rupture of the upper flange; b) rupture of the bottom flange

5.1.3. Maximum Deflection

The maximum mid-span deflection was determined for each rupture scenarios as presented in Table 10.

Table 10. Maximum mid-span deflection $\delta_{1/2span}$ (cm)

Structure without rupture		4.23
Rupture scenario	Diagonal	4.38
	Post	4.33
	Upper flange	9.12
	Bottom flange	12.20

5.2. Discussion of the Results

For the rupture of the diagonal and the upper and bottom flanges, the vibration modes and corresponding natural frequencies are very similar to the ones calculated for the structure without rupture (see Table 5). For the post's rupture, two new local modes can be observed, induced by its rupture. Table 11 presents a comparison between the stresses in the elements with maximum stress for the nominal structure, and in the same elements for each rupture scenario. As it can be observed, the rupture of the flanges corresponds to the rupture scenarios that cause the higher variations in terms of stress.

Table 11. Elements with maximum stress in the structure without rupture: variation of the stress in the rupture scenarios

	Element with maximum stress in the structure without rupture	Diagonal	Post	Upper flange	Bottom flange
Rupture scenario	Diagonal	-	1.0% (reduction)	0.6% (increasing)	0.2% (reduction)
	Post	11.0% (reduction)	-	1.8% (increasing)	0.2% (increasing)
	Upper flange	11.3% (reduction)	1.8% (reduction)	-	16.8% (increasing)
	Bottom flange	11.1% (increasing)	22.6% (reduction)	15.1% (increasing)	-

The results show that the scenarios corresponding to the rupture of the upper and bottom flanges are the ones which can put at risk the structural safety of the bridge and can cause its collapse. In both scenarios, there are elements which don't verify the structural safety condition. The computation of the corresponding safety factors clearly shows that the rupture of the upper or bottom middle flanges will certainly lead to the rupture of some diagonals. This will eventually cause the rupture of other elements and consequently the collapse of the overall structure.

The rupture of the flanges causes the higher variations of the mid-span deflection comparing to the situation of the structure without rupture: 116% for the upper flange rupture scenario and 188% for the bottom flange rupture scenario. The deformed shape for the vertical loads corresponding to the rupture of the diagonal and post are very similar to the deformed shape of the original structure. Regarding the rupture of the upper and bottom flanges, the deformed shape of the bridge for the vertical loads corresponds to a combination of vertical displacement and torsion.

6. Strengthening Solution for the S. João de Loure Bridge

External prestressing is more and more used in case of new bridge designs and in the framework of rehabilitation of old structures (Riad and Fehling 2005).

When the objective is to reduce the mid-span deflection of a bridge with similar characteristics of the reported one, the use of the strengthening solution with prestressing cables schematized in Figure 16 is very common. The model used to study the strengthening solution efficiency is the structure described in section 3, with the nominal joint stiffness.

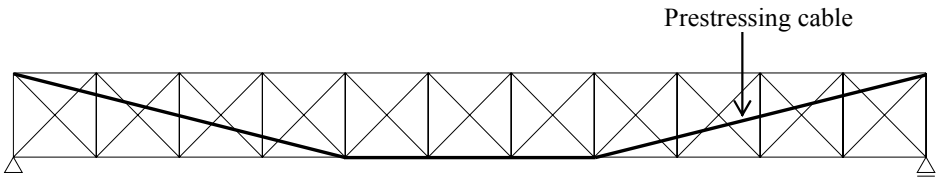

Figure 16. Strengthening scheme

6.1. Pre-stressing Simulation

To simulate the pre-stressing force, P, in each extremity of the cable (Figure 17-a), in this analysis, a negative uniform temperature variation, ΔT, was applied along the pre-stressing cables (Figure 17-b). Under a negative temperature, the cables tend to shorten, becoming tensioned as a result of the structure's opposition to that deformation.

The temperature variation was calculated using equation (10):

$$\Delta T = P \Big/ \left(E_p A_p \alpha_p \right) \tag{10}$$

Where P is the prestressing force, E_p is the Young's modulus of the prestressing steel (200 GPa), A_p is the cross-section's area of the cable (11) and α_p is the thermal expansion coefficient of the prestressing steel (1×10^{-5} /ºC).

$$A_p \geq P \big/ f_{pd} \tag{11}$$

$$f_{pd} = 0.9\left(f_{pk} \big/ 1.1 \right) \tag{12}$$

In Equation (11), f_{pd} is the design value of the prestressing cable's yielding stress, calculated from Equation (12), where f_{pk} is the characteristic value of the stress, considered equal to 1770 MPa.

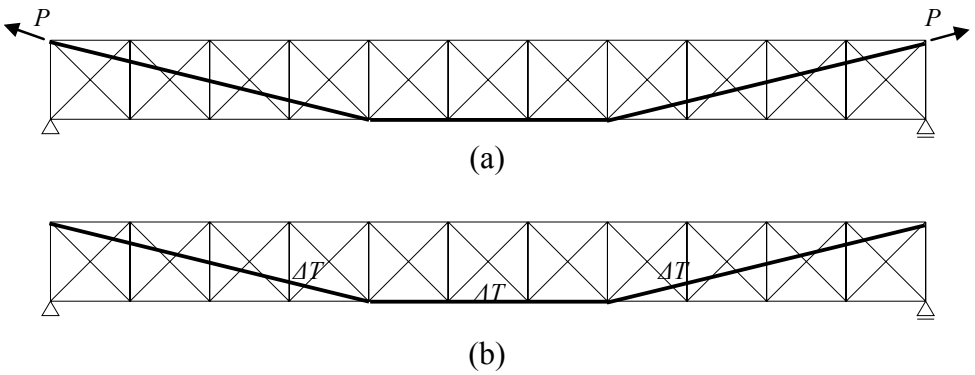

Figure 17. Pre-stressing strategies: a) Tension force, P; b) Negative uniform temperature variation, ΔT

6.2. Numerical Results

Five levels of prestressing, corresponding to five different values of ΔT and corresponding cross-section's area of the cable, A_p, were analysed (see Table 12).

Table 12. Cross-section's area (A_p) and temperatura variation (ΔT)

	Cross-section			
P (kN)	$A_p \geq$ (mm^2)	diameter (m)	A_p (mm^2)	ΔT (ºC)
700	483.36	0.030	706.858	-495.15
1400	966.73	0.040	1256.637	-557.04
2100	1450.09	0.045	1590.431	-660.20
2800	1933.46	0.055	2375.829	-589.27
3500	2416.82	0.060	2827.433	-618.94

Maximum axial forces, N_{max}, and maximum stresses, σ_{max}, in the structure's elements, and maximum mid-span deflection, $\delta_{1/2span}$, were calculated for each value of P, including $P = 0$ (original structure without prestressing). The results are presented in Table 13. Figures 18 and 19 show the evolution of the maximum axial force and maximum deflection, respectively.

Table 13. Maximum axial forces and corresponding maximum stress, and maximum deflection

P (kN)	Diagonal		Post		Upper flange		Bottom flange		$\delta_{1/2span}$ (cm)
	N_{max} (kN)	σ_{max} (MPa)	N_{max} (kN)	σ_{max} (MPa)	N_{max} (kN)	σ_{max} (MPa)	N_{max} (kN)	σ_{max} (MPa)	
0	-853.56	-86.89	-692.42	-44.44	-3416.55	-132.58	3306.61	128.31	4.23
700	-745.51	-75.89	-747.52	63.76	-3428.19	-133.03	2200.68	85.40	3.39
1400	-642.06	-65.36	-799.96	85.62	-3438.56	-133.43	1154.90	44.82	2.9
2100	-540.58	-55.03	-850.88	106.90	-3447.33	-133.77	-652.87	-25.33	1.1
2800	-560.50	-57.06	-904.45	126.57	-3458.77	-134.22	-1599.31	-62.06	1.08
3500	-819.33	-83.41	-954.42	146.20	-3467.90	-134.57	-2526.18	-98.03	0.36

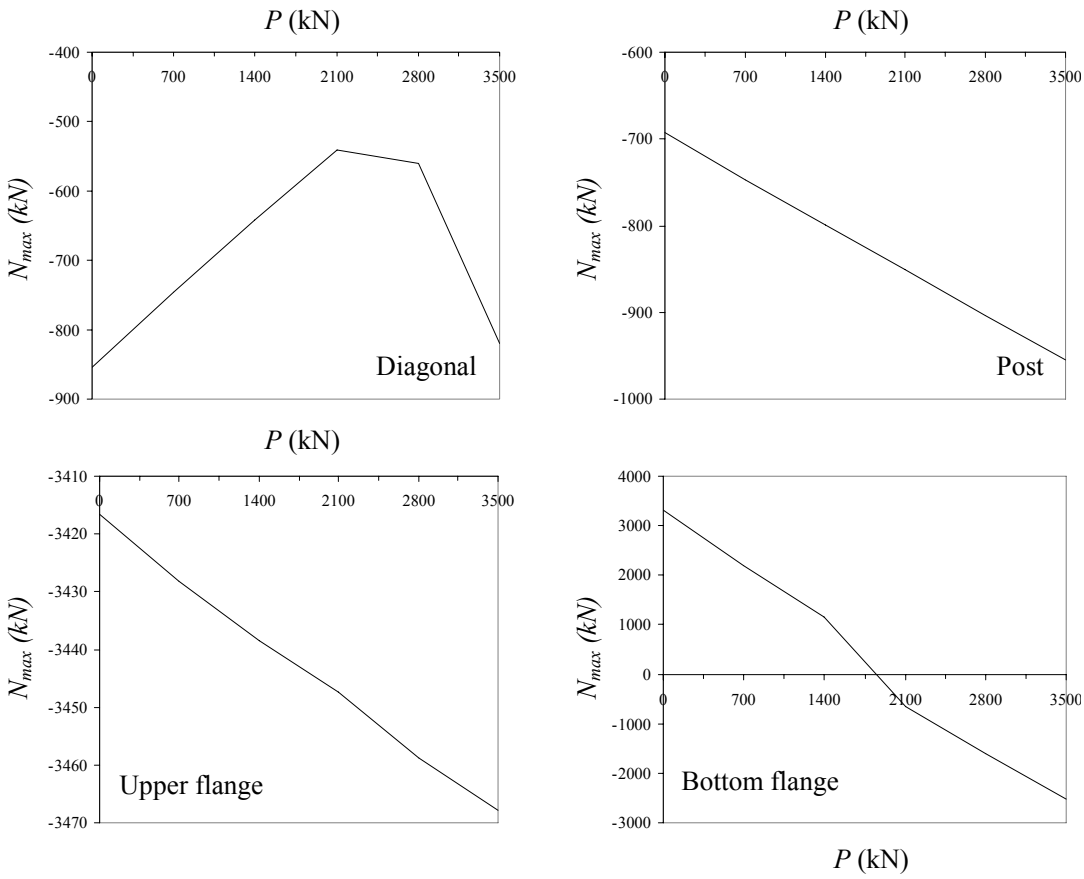

Figure 18. Maximum axial forces in the structural elements, function of *P*

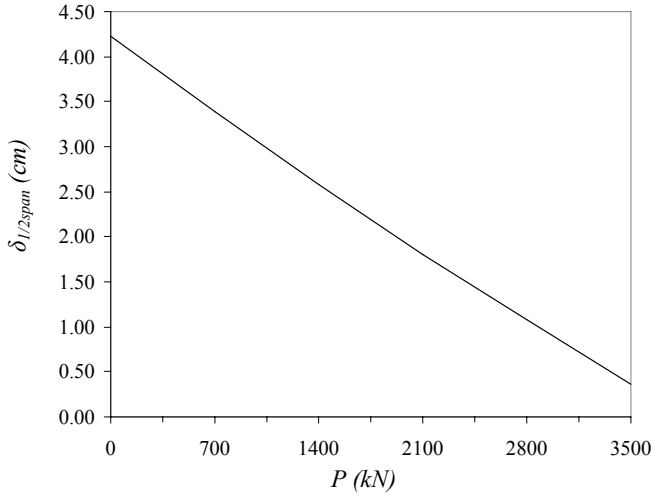

Figure 19. Maximum deflection, function of P

The maximum stress found is equal to 146.20 MPa, verifying the structural safety according to the Portuguese standard (REAE 1986). It is underlined that in these analyses, the effect of local or global instability was not considered.

$$\sigma_{max} = 146.20 \text{ MPa} < f_{yd} = 204.55 \text{ MPa} \quad (13)$$

6.3. Discussion of the Results

For a strengthening corresponding to $P = 3500$ kN:

- the maximum axial force and corresponding stress in the diagonals were reduced by 4%;
- the maximum axial force in the post was increased by 38% and the maximum stress was increased by 229%;
- the maximum axial force and corresponding stress in the upper flange were increased by 2%;
- the maximum axial force and corresponding stress in the bottom flange were reduced by 24%, from positive axial force (tension) to negative axial force (compression);
- the mid-span deflection was reduced by 91%.

7. Final Comments

From the parametric analysis of the S. João de Loure bridge, the results reveal that the joints stiffness variation, caused for example, by corrosion, has a significant influence in the structural response, mainly in terms of stress in the corresponding elements. For the stiffness variations at the joints considered in this study, the bridge structural safety in terms of stress was generally verified. Nevertheless, maintenance operations of the structural elements should be operated according to the adequate recommendations.

Regarding the analysed collapse scenarios, the rupture of the upper or bottom flanges at the middle span proved to be the worst scenarios in terms of stresses and global structure deformation. In both cases, the rupture of the element analysed, and the corresponding forces re-distribution, causes stress increases in other elements up to its strength limit. Therefore, the structural safety of the bridge can be at risk when the rupture of, at least, one of the middle flanges occurs.

Concerning the strengthening solution analysed, the numerical results showed that this simple technique is efficient in reducing the mid-span deflection. However, the internal stress

distribution is very sensitive to the value of the prestressing force adopted. The prestressing adopted in rehabilitation should be chosen as function of the bridge geometry, elements cross-sections and acting loads. For example, for the bridge under analysis, and for values of prestressing force higher than 2100 kN, the axial force in the bottom flange changes from tension to compression. For each loading case, the behaviour of the overall structure can be very different, in terms of internal stress distribution and deformations, function of the prestressing level at the strengthening cables.

Acknowledgements

The authors would like to acknowledge the Junta Autónoma de Estradas, for the information provided for this study.

References

Brinckerhoff, P. (1993), "Bridge Inspection and Rehabilitation: A Practical Guide", *John Wiley and Sons*, New York, USA.

Computer and Structures, Inc. (2003), "SAP2000 Nonlinear Ver. 8.15 User Manual", *Computer and Structures, Inc*., Berkeley, USA.

Fernandes, C. and Silva, H. (2004), "Bridges Evaluation, Maintenance and Strengthening", Department of Civil Engineering, University of Aveiro, Aveiro, Portugal,.

Fernandes, C. and Varum H. (2005), "Vulnerability Assessment of the S. João de Loure Bridge – Vouga's River", *4th International Workshop on Life-Cycle Cost Analysis and Design of Civil Infrastructure Systems*, Cocoa Beach, Florida, USA, Pages 219-227.

Freire, P.C.M., Martins, M.R.F. and Torres, M.T.P., (1998), "Steel Highway Bridges", *edited by Junta Autónoma de Estradas*, Portugal.

Furtado, A.C. and Marques, A. (2003), "Maintenance and Rehabilitation Assessment of the S. João de Loure bridge – Vouga's River", Department of Civil Engineering, University of Aveiro, Aveiro, Portugal.

Novák, B., Weiβbach, M. and Meiss, K. (2005), "Development of Deterioration Models for the Bridge Management Systems", *1st Munich Bridge Assessment Conference*, Munich, Germany.

Riad, K. and Fehling, E. (2005), "Effective Tensile Force Determination in External Pre-stressing Cables Using Vibration Measurements", *1st Munich Bridge Assessment Conference*, Munich, Germany.

REAE (1986), "Portuguese Standard for Steel Structures Design", *Decree-Law n.º 211/86*, July 31st, Edited by INCM, Lisbon, Portugal (in Portuguese).

RSA (1983), "Portuguese Standard for Safety and Loads for Buildings and Bridge Structures", *Decree-Law n.º 235/83*, May 31st, Edited by Porto Editora, Lisbon, Portugal (in Portuguese).

Varum, H., (2003), "Seismic Assessment, Strengthening and Repair of Existing Buildings", *Ph.D. Thesis*, University of Aveiro, Aveiro, Portugal.

Varum, H. and Fernandes, C. (2005), "S. João de Loure Bridge: Vulnerability Assessment and Study of a Common Strengthening Solution", *1st Munich Bridge Assessment Conference*, Munich, Germany.